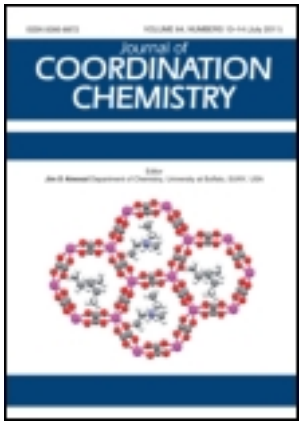

Journal of Coordination Chemistry
Publication details, including instructions for authors and subscription information:
http://www.tandfonline.com/loi/gcoo20

Comparative study of two new grid complexes: synthesis, X-ray structure characterization, thermogravimetric, and spectroscopic properties

Yuan Wang [a b], Zheng Liu [a a], Yongliao Wang [c], Jiongyang Gao [a] & Yanhong Li [d e]

[a] College of Chemical and Biological Engineering, Guilin University of Technology, Guilin 541004, PR China

[b] Center for Structural and Molecular Biology, Institute of Biophysics, Chinese Academy of Sciences, Beijing 100101, PR China

[c] College of Environmental Science and Engineering, South China University of Technology, Guangzhou 510006, PR China

[d] Guangxi Key Laboratory of Environmental Engineering, Protection and Assessment, Guilin University of Technology, Guilin 541004, PR China

[e] College of Environmental Science and Engineering, Guilin University of Technology, Guilin 541004, PR China

Published online: 05 Dec 2011.

To cite this article: Yuan Wang, Zheng Liu, Yongliao Wang, Jiongyang Gao & Yanhong Li (2011) Comparative study of two new grid complexes: synthesis, X-ray structure characterization, thermogravimetric, and spectroscopic properties, Journal of Coordination Chemistry, 64:24, 4357-4372, DOI: 10.1080/00958972.2011.639873

To link to this article: http://dx.doi.org/10.1080/00958972.2011.639873

Journal of Coordination Chemistry
Vol. 64, No. 24, 20 December 2011, 4357–4372

Comparative study of two new grid complexes: synthesis, X-ray structure characterization, thermogravimetric, and spectroscopic properties

YUAN WANG†‡, ZHENG LIU*†, YONGLIAO WANG§, JIONGYANG GAO† and YANHONG LI¶⊥

†College of Chemical and Biological Engineering, Guilin University of Technology, Guilin 541004, PR China
‡Center for Structural and Molecular Biology, Institute of Biophysics, Chinese Academy of Sciences, Beijing 100101, PR China
§College of Environmental Science and Engineering, South China University of Technology, Guangzhou 510006, PR China
¶Guangxi Key Laboratory of Environmental Engineering, Protection and Assessment, Guilin University of Technology, Guilin 541004, PR China
⊥College of Environmental Science and Engineering, Guilin University of Technology, Guilin 541004, PR China

(*Received 15 June 2011; in final form 24 October 2011*)

The synthesis and characterization of two new grid complexes, $[Ni_4(L)_4(DMF)_4]\cdot 2H_2O$ (**1**) and $[Mn_4(L)_4(DMF)_4]$ (**2**) (where L is the anion of 3,5-dichlorosalicylaldehyde pyridine-2-formyl hydrazone), were investigated. X-ray crystal structure analysis reveals that the metal centers in both complexes exhibit slightly distorted square-bipyramidal coordination geometry. The dominating interaction of two adjacent grids for **1** and **2** is Cl···H hydrogen bonds. The halogen–hydrogen bond is a key factor to stabilize the crystal structure of chloro-substituted grid compounds. Thermogravimetric curves of **1** and **2** exhibit distinct weight loss stages at different temperatures and reflect the thermal stability of the complexes. Both UV-visible and fluorescence spectra of **1** and **2** indicate they have a stronger conjugated system and the same significant quenching ability compared with H_2L. The ESI-MS spectra of **1** and **2** prove that the tetranuclear grids decompose in methanol/water solution.

Keywords: Grid complexes; Halogen-substituted; Fluorescence; Properties

1. Introduction

With progress of supramolecular coordination chemistry, a series of self-assembled compounds known as grid-like architectures were synthesized. These compounds contain 2-D arrays of metal ions which connect to a set of ligands in a perpendicular arrangement to generate a multiple linear and rigid network. These grid-type compounds can be synthesized with high yield and are thermodynamically stable and their intriguing magnetic and electronic properties make them valuable in application of

*Corresponding author. Email: lisa4.6@163.com

ISSN 0095-8972 print/ISSN 1029-0389 online
http://dx.doi.org/10.1080/00958972.2011.639873

information storage and processing technology [1–3]. Among the most widely studied ligands are poap (N^3-(2-pyridoyl)-2-pyridinecarboxamidrazone) [4–8], pahap (picolinamide azine) [6, 8], Hpop (2-(hydroxyimino)-*N*′[1-(2-pyridyl)ethylidene]propanohydrazone) [9–11], and their transition metal complexes. Grid-like complexes of poap as well as other *N*-heterocyclic derivatives [12, 13] have been studied, but there have been no reports of complexes of 2-hydroxybenzaldehyde hydrazone molecular skeletons. From the standpoint of structure, the role of halogen in the grid complex crystals is unknown. The only record of fluorescence properties of grids was reported by Cao *et al*. [13]. In all open-shell transition metal grids of derivatives from condensation of carbohydrazides and 2-phenylpyrimidine-4,6-dicarbaldehyde, only Zn^{2+} grids have quenching phenomena [13]. However, an important bioelement, Mn^{2+}, as reflected in Irving–Williams sequence, has not had fluorescence reported due to oxidation complexity and relatively low stability of its complexes.

In this contribution, based on the fact that hydrazine can form mononuclear, dinuclear [8], tetranuclear or even multinuclear [7] coordination features, we synthesized chloro-substituted 2-hydroxybenzaldehyde acylhydrazone H_2L (scheme 1) and two new grid-like complexes, which in combination with the salicyl groups may enhance their anti-inflammatory activity [14]. Comparison of X-ray crystal structures, thermogravimetric (TG) analysis, electronic spectroscopic studies and fluorescence properties of the two complexes are reported. In particular, we discuss the characteristics of halogen–hydrogen bonds between adjacent lattices and the differences between solvent with axial coordination in two grids by TG curves. To the best of our knowledge, this report is the first to study the TG properties of grids and fluorescence for Ni^{2+}, Mn^{2+} lattice complexes.

2. Experimental

2.1. *Materials*

All reagents and solvents were purchased from commercial sources and used as received.

2.2. *Methods*

Solution ^{1}H (500 MHz) nuclear magnetic resonance (NMR) spectra were recorded with a Bruker Ultrashield Avance DRX-500 instrument using residual solvent proton

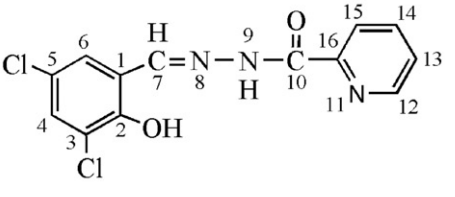

Scheme 1. Schematic drawing of ligand H_2L.

resonances as internal reference for the ^{1}H NMR. Elemental analysis for C, H, and N was performed on a Vario EL elemental analyzer. IR spectra were recorded on a Shimadzu FTIR-8400 using KBr pellets. Thermal stability analyses were performed on a Netzsch STA-449 instrument in N_2 with a heating rate of 10°C min^{-1}. UV-Vis spectra were obtained in anhydrous DMF with a Shimadzu UV-2450 Spectrophotometer. Luminescence measurements were carried out on a Perkin Elmer LS-45/55 Fluorescence Spectrophotometer. High-resolution mass spectra were obtained on an Agilent 6100 Single Quadropole system equipped with an Agilent 1200 LC module (Agilent, Santa Clara, USA), and with an electrospray ionization source. The mass spectrometer was operated in the positive ion mode. Single-crystal samples of **1** and **2** were washed with acetonitrile and methanol, respectively, dried under vacuum and then ground by agate mortar for 1 h.

2.3. *X-ray structure determination*

X-ray diffraction data for single crystals of **1** and **2** (**1**, $0.32 \times 0.16 \times 0.13$ mm; **2**, $0.17 \times 0.15 \times 0.08$ mm) were collected at 293(2) K on a Bruker Smart CCD system equipped with monochromated Mo-Kα radiation ($\lambda = 0.71073$ Å) using the ω–ϕ scan technique. Data integration and empirical absorption corrections were performed by *SAINT* programs [15]. The structures were solved by direct methods using SHELXS-97 [16] and refined by full-matrix least-squares on F^2 using SHELXL-97 [17]. All atoms except hydrogen were refined anisotropically.

2.4. *Synthesis of the ligand H_2L*

H_2L was obtained from the hydrazide reaction of pyridine-2-carboxylic acid methyl ester and hydrazine followed by condensation of 3,5-dichlorosalicylaldehyde and 2-picoloylhydrazine, prepared according to published procedures [18, 19]. The compound was recrystallized from boiling ethanol by cooling on ice (yield: 87%). Anal. Found: C, 50.17; H, 2.98; N, 13.55. Calcd for $C_{13}H_9N_3O_2Cl_2$ (%): C, 50.22; H, 2.92; N, 13.51. ^{1}H NMR (500 MHz, DMSO-d_6) (ppm): $\delta = 12.89$(s, 1H, OH), 12.57(s, 1H, ^{9}NH), 8.09–8.06(m, 1H, ^{7}CH), 8.80(s, 1H, ^{12}CH), 8.15(d, 1H, $J = 7.75$Hz, ^{13}CH), 8.74(d, 1H, $J = 4.05$Hz, ^{14}CH), 7.71–7.69(m, 1H, ^{15}CH), 7.57(d, 1H, $J = 2.15$Hz, ^{4}CH), 7.63(d, 1H, $J = 2.2$Hz, ^{6}CH). IR(KBr pellet, cm^{-1}): 1592(s), 3068(m), 3264(s), 1676(s), 1513(s), 1454(s), 1439(s), 1184(m), 1222(m), 1272(m), 1000(m), 736(m).

2.5. *Synthesis of $[Ni_4(L)_4(DMF)_4] \cdot 2H_2O$ (1)*

An anhydrous methanol solution (10 mL) of $Ni(NO_3)_2 \cdot 6H_2O$ (0.5 mmol, 0.145 g) was slowly added to a stirred slurry of H_2L (0.5 mmol, 0.155 g) in methanol (15 mL) at 65°C gave a grass green solution; 45 min later, with 6 drops of concentrated ammonia, the pH of the solution was adjusted to between 7 and 8. Copious precipitation of brown solid occurred immediately. The solution was equilibrated for 1.5 h and then filtered. The residue was dissolved in DMF (20 mL) and the solution was filtered to remove a small amount of gelatinous material. The solution was mixed with same volume of anhydrous acetonitrile. Brown stripe single crystal was formed several days later by slow

evaporation at room temperature (yield: 73%). Anal. Found: C, 42.72; H, 3.14; N, 12.65. Calcd for $C_{64}H_{60}Cl_8N_{16}Ni_4O_{14}$ (%): C, 42.81; H, 3.37; N, 12.48. IR(KBr pellet, cm^{-1}): 1606(s), 1651(s), 2925(w), 3054(w), 1159(m), 1537(s), 1479(s), 1444(s), 3646(w), 3585(w), 1594(m), 1209(m), 752(m).

2.6. *Synthesis of [$Mn_4(L)_4(DMF)_4$] (2)*

A distilled water solution (10 mL) of $MnCl_2 \cdot 4H_2O$ (0.5 mmol, 0.099 g) was slowly added to a stirred slurry of H_2L (0.5 mmol, 0.155 g) in anhydrous methanol (15 mL) at 65°C and gave a turbid yellow solution; 45 min later, with 8 drops of triethylamine, the pH of the solution was adjusted to between 7 and 8. After 1.5 h, red-brown precipitate appeared and the solution was filtered. The residue was dissolved in DMF (40 mL), filtered to remove a small amount of gelatinous material and the solution was mixed with same volume of anhydrous methanol. Red block single crystals were formed several days later by slow evaporation at room temperature (yield: 68%). Anal. Found: C, 44.14; H, 3.29; N, 12.78. Calcd for $C_{64}H_{56}Cl_8N_{16}Mn_4O_{12}$ (%): C, 44.06; H, 3.24; N, 12.85. IR(KBr pellet, cm^{-1}): 1601(s), 3401(s), 1653(s), 2929(w), 3072(w), 1156(m), 1535(s), 1475(s), 1452(s), 1581(s), 1207(m), 755(m).

Details of the crystal parameters, data collection, and refinements for **1** and **2** are summarized in table 1. Selected bond lengths and angles for **1** and **2** are listed in table 2.

3. Results and discussion

3.1. *X-ray crystallography*

3.1.1. $[Ni_4(L)_4(DMF)_4] \cdot 2H_2O$ (1). The results of crystal structure analysis reveal that **1** is a centrosymmetric configuration. From bond lengths (table 2) and figure 1, each Ni^{2+} is coordinated by two mutually perpendicular enol-type L^{2-} (scheme 2) and one solvent DMF to form repeating units, while two water molecules dissociate from the lattice. The molecule is electroneutral. Ni1 and Ni1A have the same slightly distorted tetragonal-bipyramid coordination mode, each six-coordinate by three nitrogen atoms, two oxygen atoms from L, and one oxygen atom from DMF. Similarly, Ni2 (Ni2A) is coordinated by two nitrogen atoms, three oxygen atoms from L, and one oxygen atom from DMF. These atoms around each metal form two five-membered rings and one six-membered ring. The acyl oxygen atoms and hydrazide (–N–N–) are bridge. Bridge angle Ni1–O3–Ni2A (Ni1A–O3A–Ni2) is 140.682(6)°, close to 139.08(10)° reported by Matthews *et al.* [5]. Torsion angle Ni1–N2–N3–Ni2 (Ni1A–N2A–N3A–Ni2A) is 159.221(8)°. For Ni1, the equatorial plane is defined by O3, N6, O4, N2, and the apical positions are occupied by N1, O5, while Ni1 deviates from the tetragonal plane by 0.0232 Å toward O5. For Ni2, the equatorial plane is defined by O1, N3, O2, N4A and the apical positions are occupied by O3A, O6, while Ni2 deviates from the tetragonal plane by 0.0045 Å toward O3A.

As shown in figure 1, four nickels are arranged in an approximate rectangle. Each nickel is in the least-squares plane, indicating the complex is a highly symmetrical, in which the shorter edge (Ni1(Ni1A) ··· Ni2A(Ni2)) length (3.9015(4) Å) is close to 3.91 Å

Table 1. Crystallographic data for **1** and **2**.

Complex	**1**	**2**
Formula	$C_{64}H_{60}CL_8N_{16}N_{14}O_{14}$	$C_{64}H_{56}CL_8N_{16}Mn_4O_{12}$
Formula weight	1795.72	1744.62
Crystal system	Triclinic	Triclinic
Space group	$P\bar{1}$	$P\bar{1}$
Unit cell dimensions (Å, °)		
a	12.3311(13)	12.6472(12)
b	12.7538(15)	12.6975(13)
c	13.4979(18)	13.6241(15)
α	70.8120(10)	102.8770(10)
β	66.5230(10)	94.6730(10)
γ	88.552(2)	119.686(2)
Volume (Å^3), z	1825.2(4), 1	1804.7(3), 4
Calculated density (g cm^{-3})	1.634	1.605
μ (mm^{-1})	1.383	1.052
R_{int}	0.0894	0.0558
$R_1(I > 2\sigma(I))$[a]	0.0909	0.0683
wR_2 (all data)[b]	0.2399	0.1796
Goodness-of-fit on F^2	1.007	1.028

[a] $R_1 = \sum||F_o|-|F_c||/\sum|F_o|$, [b] $wR_2 = [\sum w(F_o^2 - F_c^2)^2/\sum w(F_o^2)^2]^{1/2}$.

Table 2. Selected bond lengths (Å) and angles (°) for **1** and **2**.

1					
Ni1–N1	2.051(9)	Ni2–N3	1.987(8)	C1–N2	1.310(13)
Ni1–N2	2.060(8)	Ni2–N4A	2.020(8)	N2–N3	1.391(10)
Ni1–N6	1.973(8)	Ni2–O1	2.051(7)	N3–C7	1.278(12)
Ni1–O3	2.055(7)	Ni2–O2	1.991(7)	C14–N5	1.281(12)
Ni1–O4	1.996(8)	Ni2–O3A	2.088(7)	N5–N6	1.396(11)
Ni1–O5	2.225(8)	Ni2–O6	2.142(9)	N6–C20	1.294(13)
N1–Ni1–O5	175.2(3)	O4–Ni1–N2	92.3(3)	O2–M2–N4A	96.4(3)
N2–Ni1–O3	98.3(3)	O3A–Ni2–O6	167.9(3)	N4A–Ni2–O1	94.4(3)
O3–Ni1–O6	79.8(3)	O1–Ni2–N3	78.9(3)		
N6–Ni1–O4	89.8(3)	N3–Ni2–O2	90.4(3)		
2					
Mn1–O1	2.047(5)	Mn2A–O3A	2.085(5)	C1–N1	1.262(8)
Mn1–O2	2.157(5)	Mn2A–O4A	2.189(5)	N1–N2	1.385(7)
Mn1–O4	2.173(5)	Mn2A–O6A	2.262(5)	N2–C8	1.314(8)
Mn1–O5	2.229(5)	Mn2A–N2	2.205(5)	C14–M4	1.268(9)
Mn1–N1	2.250(5)	Mn2A–N3A	2.241(6)	N4–N5	1.393(7)
Mn1–N6	2.254(5)	Mn2A–N4A	2.238(6)	N5–C21	1.284(8)
O4–Mn1–O5	156.97(18)	N6–Mn1–O1	122.23(19)	O6A–Mn2A–N4A	84.4(2)
O1–Mn1–N1	82.03(19)	O3A–Mn2A–O4A	146.1(2)	N4A–Mn2A–N2	121.2(2)
Nl–Mn1–O2	71.81(19)	N2–Mn2A–N3A	73.6(2)		
O2–Mn1–N6	84.14(19)	N3A–Mn2A–O6A	83.6(2)		

in previous study [5]. The shorter edge distance is less than the sum of Ni $\cdots$ Ni van der Waals radii (4.00 Å), showing weak interactions between the short side of the metal ions may exist.

Complex **1** comprises two sets of π–π stacking phenomena (figure 2), each π–π stack includes a benzene ring (C8, C9, C10, C11, C12, C13) of acylhydrazone and another

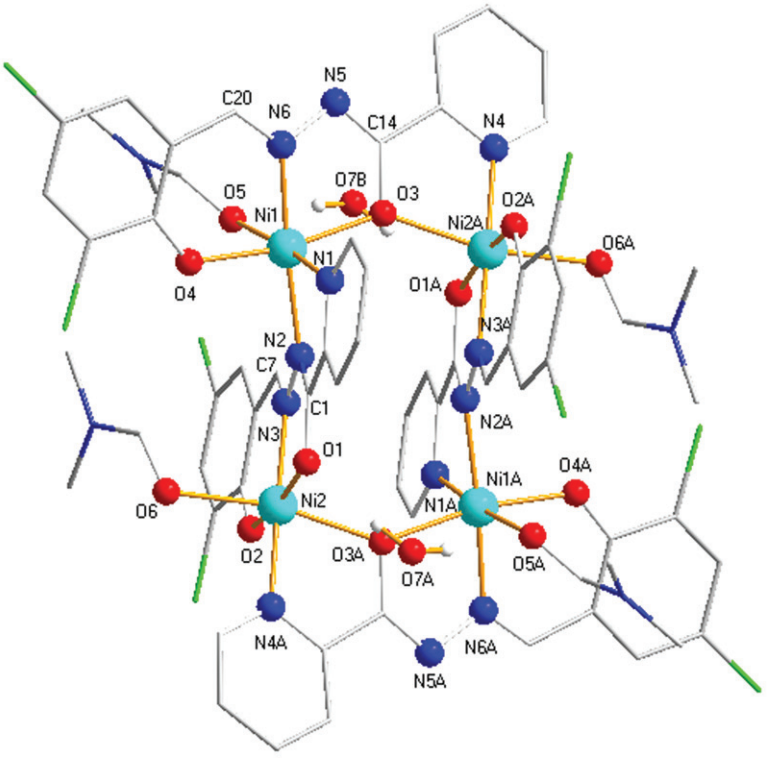

Figure 1. Diamond drawing of $[Ni_4(L)_4(DMF)_4]\cdot 2H_2O$. Hydrogen atoms were omitted for clarity.

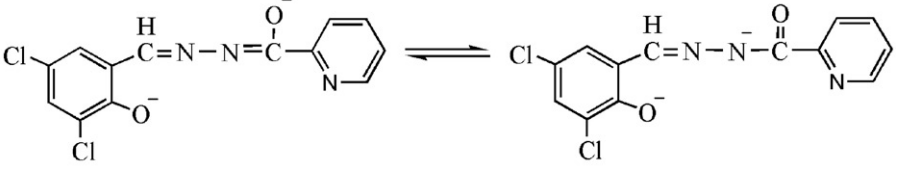

Scheme 2. Schematic drawing of tautomeric form for L^{2-}.

pyridine ring (N1, C2, C3, C4, C5, C6). The dihedral angle of two ring planes is 4.4°, which indicates an almost exactly face to face overlap. The center distance is Cg1···Cg2 3.5548(3) Å (table 3). The interactions of a pair of longer edges of contiguous grid (namely the interactions between chlorides of one grid and the adjacent grid DMF methyl H) is 2.9733(3) Å (H29B···Cl2). The shorter sides of the adjacent lattice have four pairs of interactions (figure 3), and they are H6···N5 3.0804(3) Å, H20···Cl1 3.0216(4) Å, H26···Cl1 3.0169(3) Å, and H26···Cg3 3.0089(3) Å (Cg3: N4, C15, C16, C17, C18, C19). As the essential molecular features, centrosymmetric aryl C–H···N dimer was simple and general in a diquinoline derivative reported by Marjo *et al.* [20]. A subsequent statistical analysis, using the Cambridge Structural

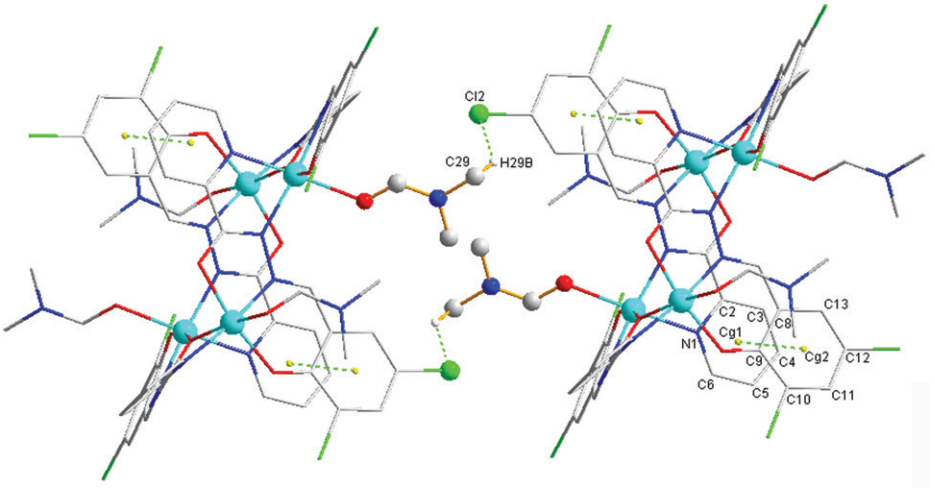

Figure 2. View of the interactions between longer edges of two adjacent grids for **1** depicted as broken green lines.

Table 3. Hydrogen-bond data (Å and °) for **1** and **2**.

D–H···A	*d*(D–H)	*d*(H···A)	*d*(D···A)	∠DHA
1				
C6–H6···N5[a]	0.9300(1)	3.0804(3)	3.9819(4)	163.780(12)
C20–H20···Cl1[b]	0.9300(1)	3.0216(4)	3.4256(4)	108.032(10)
C26–H26···Cl1[b]	0.9300(1)	3.0169(3)	3.4322(3)	108.857(10)
C26–H26···Cg3[c]	0.9300(1)	3.0089(3)	3.3467(3)	103.243(9)
C29–H29B···C12[d]	0.9600(1)	2.9733(3)	3.7229(3)	135.871(10)
Cg1···Cg2[c]	–	3.5548(3)	–	–
2				
Cl1–H11···C12[e]	0.9300(1)	2.7847(2)	3.7052(3)	170.565(11)
Cg4···Cg5[c]	–	3.4789(3)	–	–

Symmetry codes: [a]: $1-x, -y, 1-z$; [b]: $x, y-1, z$; [c]: x, y, z; [d]: $1-x, 1-y, -z$; [e]: $2-x, 4-y, 2-z$. Cg1=C2, C3, C4, C5, C6, N1; Cg2=C8, C9, C10, C11, C12, C13; Cg3=C15, C16, C17, C18, C19, N4; Cg4=C2, C3, C4, C5, C6, C7; Cg5=C9, C10, C11, C12, C13, N3.

Database (CSD), of C–H···N interactions show that they exist in the reported structures with H···N distances shorter than 2.45 Å (van der Waals sum 2.75 Å) and with a mean C–H···N angle of $120 \leq \alpha \leq 180°$ [21]. Thallapally and Nangia defined a C–H···Cl contact as either short, medium, or long using the criteria <2.6 Å, 2.6–3.0 Å, and >3.0 Å, respectively [22]. On closer inspection of these four pairs of interactions, the pair of H···N interactions (H···N 3.0804(3) Å, ∠C–H···N is 163.78°) are weak. The two pairs of H···Cl bonds (H20···Cl1 3.0216(4) Å, H26···Cl1 3.0169(3) Å) belong to a relatively stronger interaction and the C–H···π interactions provide an extra source of stability.

Thus, while strong halogen–hydrogen bonds play a central role between the two grids, the combined influence of weak interactions is also evident in the structures.

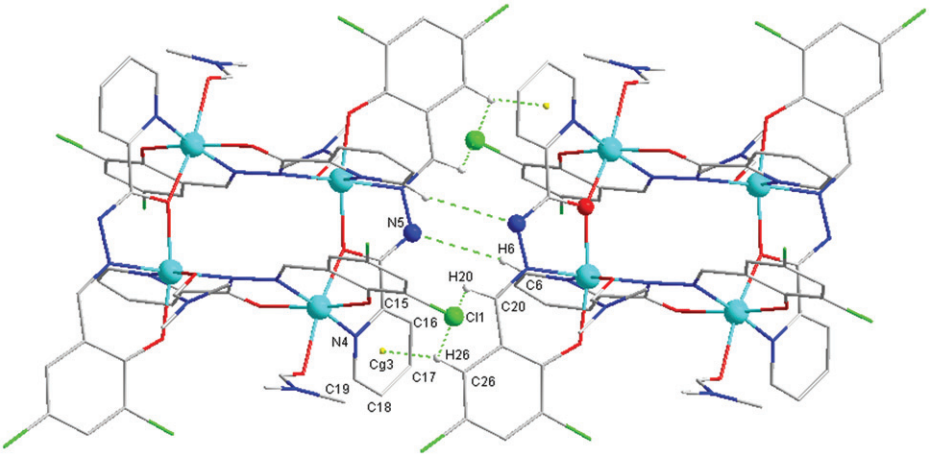

Figure 3. View of the interactions between shorter edges of two adjacent grids for **1** depicted as broken green lines.

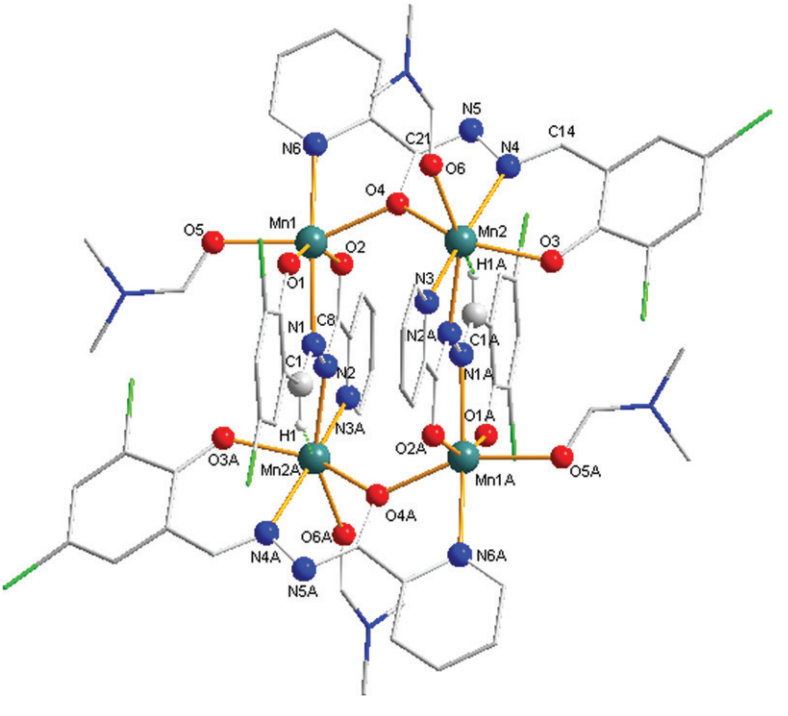

Figure 4. Diamond drawing of $[Mn_4(L)_4(DMF)_4]$. Hydrogen atoms were omitted for clarity.

3.1.2. $[Mn_4(L)_4(DMF)_4]$ (2). Complex **2** has the same crystal system and space group compared with complex **1**, but their cell parameters have notable differences. Similar to **1**, H_2L in **2** with doubly deprotonated enol-type structure L^{2-} coordinates to Mn (figure 4). O1, N1, O2, and N6 around Mn1 form the equatorial plane, while DMF and an oxo bridge are in the axial positions; Mn1 deviates from the best-fit plane by

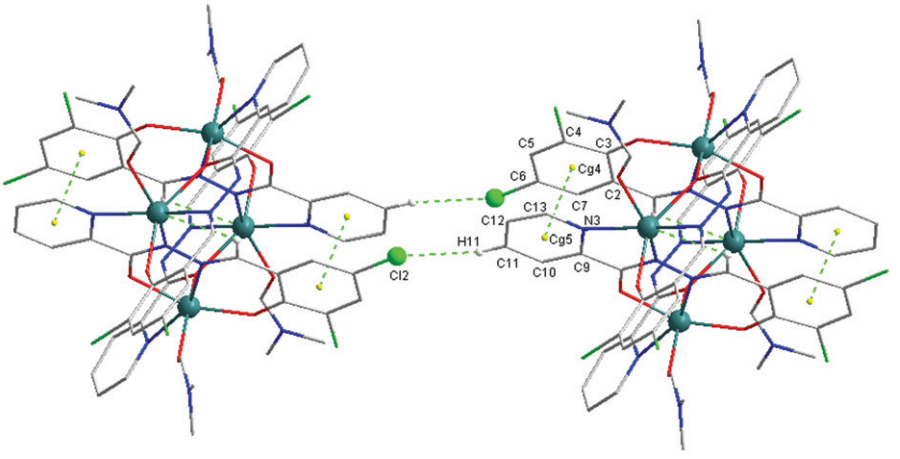

Figure 5. View of the interactions between shorter edges of two adjacent grids for **2** depicted as broken green lines.

0.0072 Å toward O4. Different from Ni^{2+} of **1** and Mn1 (Mn1A) of **2**, DMF is not in apical positions around Mn2 (Mn2A), which deviates 0.0213 Å from the equatorial plane (N2, N3A, N4A, O6A). The average axial length of 2.169(5) Å in **2** is 0.245 Å, which is longer than the average Mn–O/N distance of 1.924 Å in the equatorial plane [23] from Jahn–Teller effects. The Jahn–Teller projections of Mn1 (Mn1A) and Mn2 (Mn2A) within **2** are not mutually collinear because of the presence of two symmetry-independent species. Bridge angle Mn1–O4–Mn2 (Mn1A–O4A–Mn2A) 128.053(7)° is close to 119.7–128.8° in Mn_{16} grid prepared by Dey *et al*. [24]. Torsion angle Mn1–N1–N2–Mn2A (Mn1A–N1A–N2A–Mn2A) is 165.374(8)°. Different structures of the two grids were determined by free rotation of mono-coordinated hydrazide N4–N5(N4A–N5A) in **2** and N5–N6 (N5A–N6A) in **1** [25]. The distance H1···Mn2 (2.8658(3) Å) and angle C1–H1–Mn2 (121.515(10)°) indicate a pair of weak H···M interactions in the grids [26]. Of note is the fact that all of the coordination bond lengths of **2** are shorter than those of **1**, and more uneven distribution of coordination bond angles of **2** compared to **1** (table 2), suggesting that L anion better matches with Ni^{2+}.

Four manganese ions are arranged in an approximate rectangle, while each manganese is on their least-squares plane, in which the shorter edge (Mn1(Mn1A)···Mn2A(Mn2)) length (3.9216(3) Å) and the longer edge (Mn1(Mn1A)···Mn2(Mn2A)) length (5.2674(4) Å) approach to 3.930 Å and 5.290 Å, respectively, reported by Thompson *et al*. [27]. The length of the shorter edge is less than the sum of Mn···Mn van der Waals radii (4.10 Å), showing that weak interactions between the short side of the metal ions might exist.

As in **1**, there are also π–π stacking interactions in **2**, including a benzene ring and a pyridine ring. In figure 5, the dihedral angle of two ring planes (C2, C3, C4, C5, C6, C7; N3, C9, C10, C11, C12, C13) is 3°, almost exactly face to face overlap. The center distance Cg4···Cg5 is 3.4789(3) Å, highlighting the importance of π stacking forces by "seizing" a molecule in proximity to a metal ion site. Maximization of stabilizing π–π contacts between ligands, the rigid conjugated structure of enol-type (–C=N–N=CO–) and balance of the coordination algorithms of the metals lead to all ligands in **1** and **2**

adopting a fairly flat overall conformation. In the packing of the Mn_4 grid, the interactions which belong to moderate hydrogen bonds of the adjacent shorter side (H11 $\cdots$ Cl2 2.7847(2) Å) are the only directional stabilization of the connection between lattices.

Compounds **1** and **2** are not same as a consequence of the coordination ability of metal combined with the different bridge angles (M–O–M) and torsion angles (M–N–N–M). However, there are several structural similarities between **1** and **2**; most important, chlorides as substituent groups have some influence in promoting stacking of **1** and **2**, which is a driving force for intermolecular recognition.

3.2. *TG analysis*

The TG analysis of **1** exhibits three continuous weight loss stages: first releasing all lattice water molecules below 82°C, then on heating from 82°C to 396°C release of coordination DMF (Found 15.87, Calcd 16.61%), the ligand decomposes completely at 361°C (figure 6). Simultaneously in one temperature range **1** loses its four DMF molecules (figure 7), indicating that their chemical environments are identical. However, **2** only releases two DMF molecules below 355°C (Found 8.61, Calcd 8.37%) (figure 8) and there is no clear mass loss plateau of the other two-coordinated DMF. The fact that the four-coordinated DMF molecules dissociate at different temperatures indicates strength difference of the interaction between DMF and $[Mn_4(L)_4]$. Qin *et al.* found similar TG phenomena for $[Ba(DMF)_2(H_2O)]_2[Mo_8O_{26}]\cdot 2DMF$ also releasing coordinated DMF step by step [28].

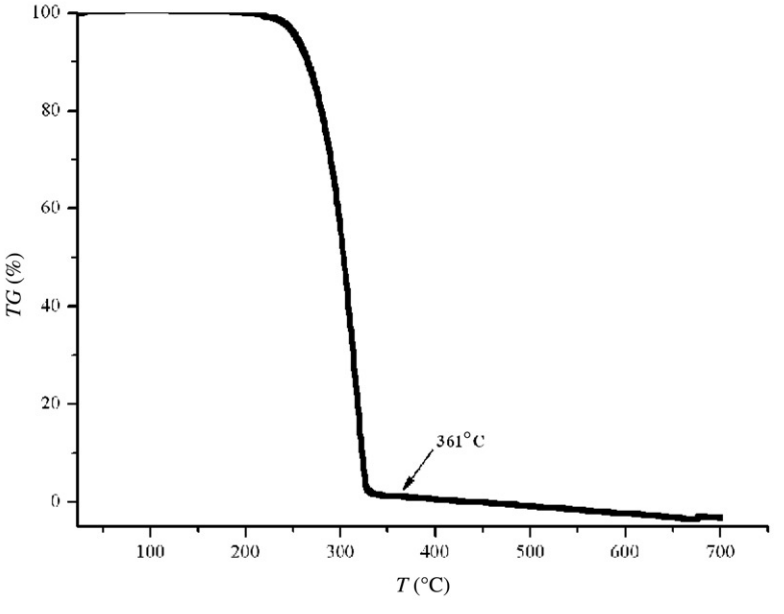

Figure 6. TG chart of the ligand H_2L.

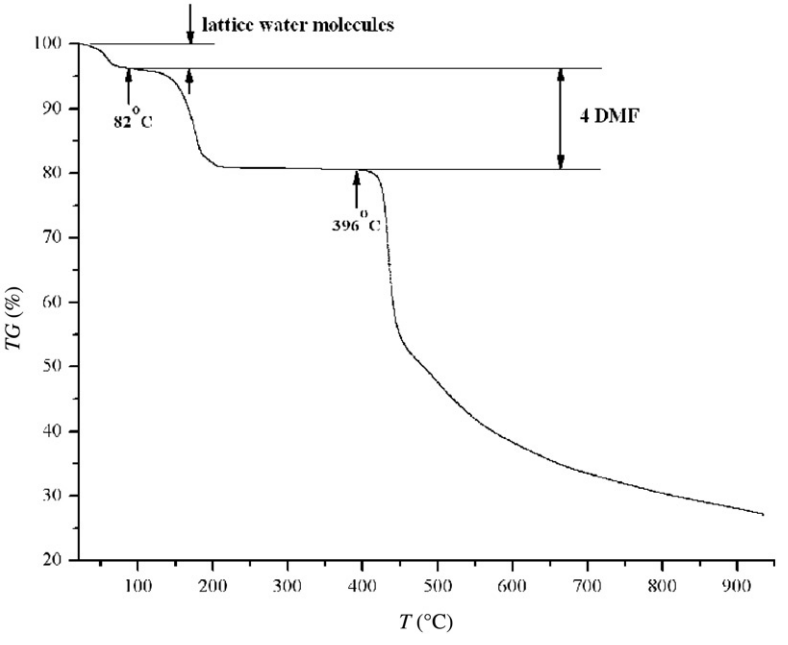

Figure 7. TG chart of **1**.

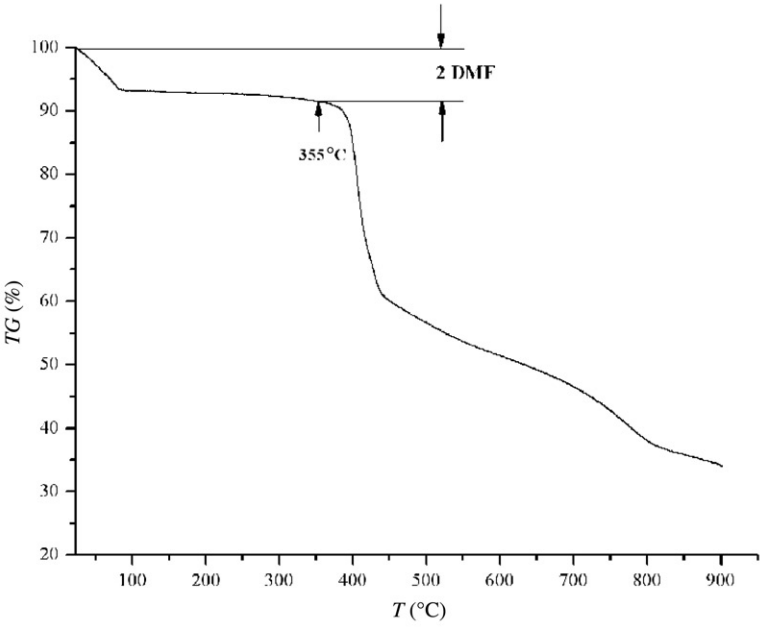

Figure 8. TG chart of **2**.

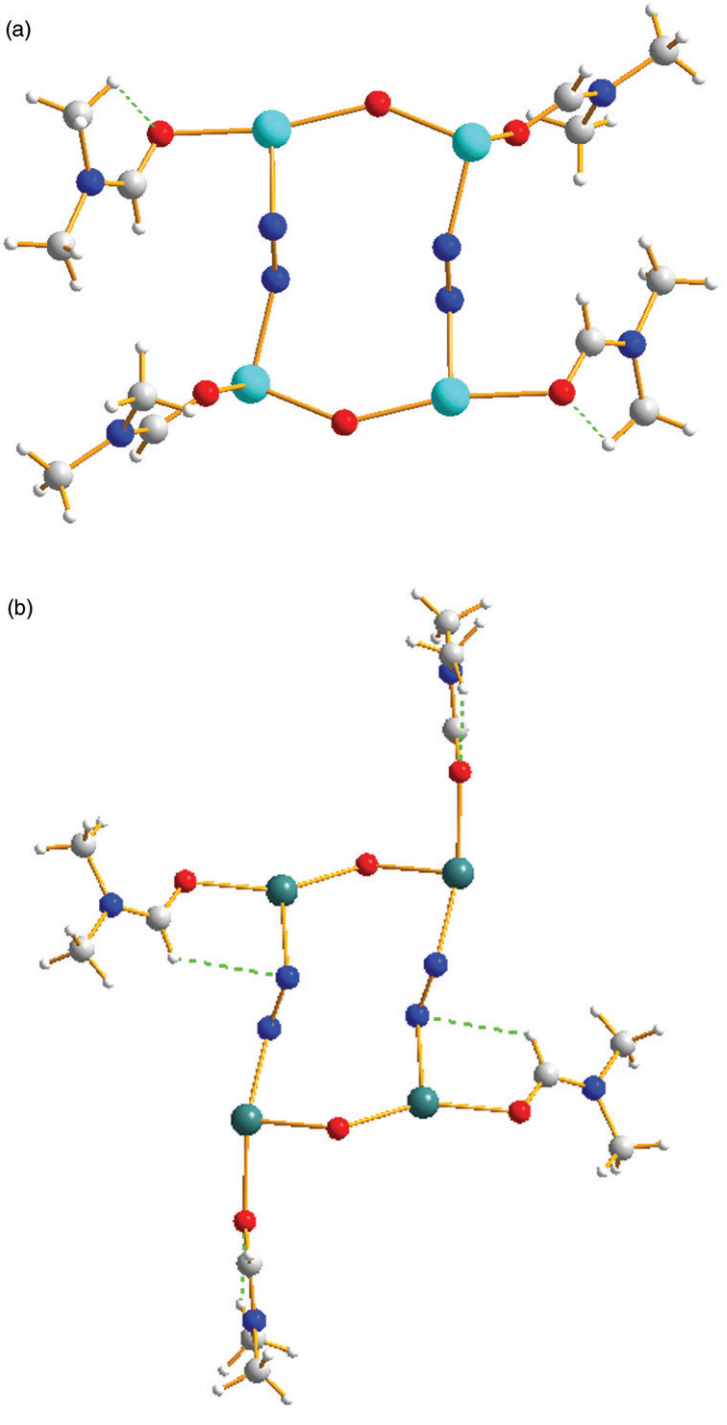

Figure 9. Distribution of DMF in **1** and **2**.

Although coordination of **1** and **2** are similar, the arrangement of four coordinated DMF molecules is completely different, which is the major reason for different DMF mass loss curves (figure 9). L^{2-} coordinated to Ni^{2+} ions are a better fit and can form a more symmetrical molecule than Mn^{2+} ions. The final mass loss percentage composition of **1** and **2** at 900°C are 27.00% and 33.97%, respectively. Neither reaches constant weight and decomposition is still going on.

3.3. *UV-Vis and luminescence*

The solution UV-Vis spectrum of H_2L (figure 10) has maxima responses at 409 nm ($\varepsilon = 175$), 338 nm ($\varepsilon = 1105$), 309 nm ($\varepsilon = 2025$), 296 nm ($\varepsilon = 2068$), and 263 nm ($\varepsilon = 1138$). The absorption spectra of complexes show three bands, **1** at 426 nm ($\varepsilon = 5650$) and **2** at 421 nm ($\varepsilon = 6320$) (Band 1 are assigned to $^3T_{1g} \leftarrow {}^3A_{2g}$ transitions for an octahedral environment [29]). Band 1 is expected to be sensitive to the nature of the axial ligand DMF [30, 31]. Band 2 of **1** and **2** display two clear absorptions at 334 nm ($\varepsilon = 3340$) and 329 nm ($\varepsilon = 6210$), respectively, attributed to metal-ligand charge transfer. They exhibit blue-shift compared with the free ligand absorption at 338 nm. The molar absorption coefficient of **2** at 329 nm is nearly twice as much as **1** at 334 nm, showing that reductive capacity of Mn ions are stronger than Ni ions. Compared with the ligand, complexes have high-intensity absorption above 300 nm, suggesting large conjugated system. The third band, **1** at 267 nm ($\varepsilon = 6450$) and **2** at 266 nm ($\varepsilon = 5280$), both have strong absorption due to the n–π^* transition in the ligands. Despite the UV spectra shape of **1** and **2** being similar, the maximum absorption of **1** is at 267 nm, while

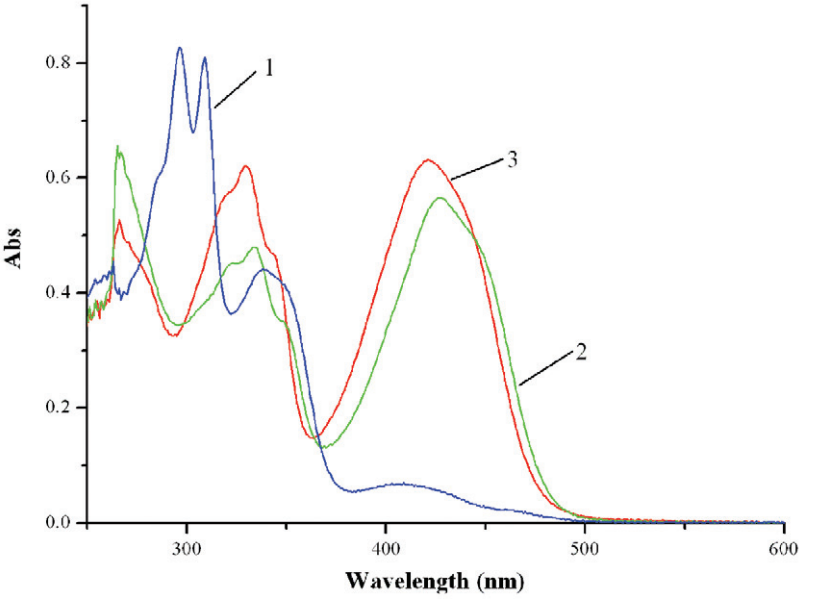

Figure 10. Room temperature UV spectra of H_2L (line 1, 4×10^{-5} mol L^{-1}), **1** (line 2, 1×10^{-5} mol L^{-1}) and **2** (line 3, 1×10^{-5} mol L^{-1}) in DMF.

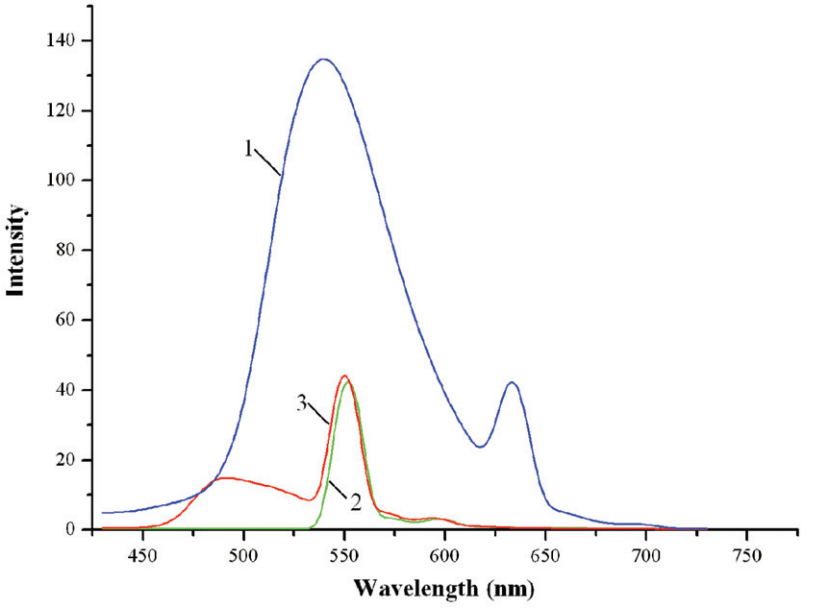

Figure 11. Room temperature fluorescence emission spectra of H_2L (line 1, 4×10^{-5} mol L^{-1}), **1** (line 2, 1×10^{-5} mol L^{-1}) and **2** (line 3, 1×10^{-5} mol L^{-1}) in DMF.

that of **2** is at 421 nm. ESI-MS spectra prove that neither **1** nor **2** exists with tetranuclear grid coordination in methanol/water ($V_{methanol} : V_{water} = 80 : 20$) solution (for solubility plus ESI compatibility), which is different from $[Cu_2Mn_2(pop)_4(OAc)_4] \cdot 7H_2O$ reported by Moroz *et al.* [9]. The difference is mainly due to the axial DMF molecules in grids replaced by more polar water, which leads to tetranuclear lattice transforming into mono- or di-nuclear complexes.

At room temperature, the comparison of fluorescence emission spectra for H_2L, **1** and **2** is given in figure 11. Fluorescence data were collected in DMF with fluorophore concentrations of 1×10^{-5} mol L^{-1}. Around 540 nm is a fluorescence peak which is generated by the ligand structure itself, and the fluorescence peak position of **1** is consistent with **2**. A comparison of the three spectra (figure 11) reveals significant quenching of the emission intensity of **1** and **2**. Because of the conjugated enol-type hydrazone in complexes, each metal is connected with a pyridine ring and benzene ring. After formation of complexes, the overall grids become larger conjugated clusters. Raising the conjugated degree of π electrons enhances the delocalization of π electrons, reducing the energy barrier required by system transition and the conjugated system. Increasing the rigidity of plane weakens the vibration of molecules so that the excited energy of molecules cannot be easily released by thermal energy.

4. Conclusions

Halogen–hydrogen interactions are the least studied variety of weak hydrogen bonds and in this work we have an experimental approach to the nature of these interactions

in grid complexes. Herein, we designed and prepared two grid complexes, $[Ni_4(L)_4(DMF)_4]\cdot 2H_2O$ (**1**) and $[Mn_4(L)_4(DMF)_4]$ (**2**), with H_2L (3,5-dichlorosalicylaldehyde pyridine-2-formyl hydrazone). X-ray crystal structures reveal that they have very similar configuration. In **1** and **2**, intermolecular C–H $\cdots$ Cl hydrogen-bonding interactions result in a 2-D network and a 3-D supramolecular assembly, respectively. Chlorides as substituent groups have some influences on promoting the stacking of complexes, which is a driving force for intermolecular recognition.

The properties of two grids are compared herein. Neither **1** nor **2** exists with tetranuclear grid coordination in methanol/water solution. Their UV-Vis spectra and fluorescence emission spectra at room temperature have a similar pattern, which leads to significant quenching of the emission intensity compared to H_2L. Their distinctly different TG analyses suggest that the coordinated DMF in **1** and **2** possess different chemical environments. Clearly, L combining with Ni^{2+} is more symmetrical than that of **2**, which is consistent with the difference of their crystal structure.

Supplementary material

Crystallographic data (excluding structure factors) for the structures reported in this article have been deposited with the Cambridge Crystallographic Data Center as Supplementary Publication Nos CCDC-724385 (**1**) and CCDC-724386 (**2**). Copies of the data can be obtained free of charge on application to CCDC, 12 Union Road, Cambridge CB2 1EZ, UK, Fax: +44 1233 336 033; E-mail: deposit@ccdc.cam.ac.uk.

Acknowledgments

The authors thank the Key Laboratory of Environmental Engineering, Protection, and Assessment of Guangxi, the National Water Pollution Control and Management of China (No. 2008ZX07317-02), and the Program to Sponsor Teams for Innovation in the Construction of Talent Highlands in Guangxi Institutions of Higher Learning (GuiKeRen 2007-71) for the financial support.

References

[1] M. Ruben, J. Rojo, F.J. Romero-Salguero, L.H. Uppadine, J.M. Lehn. *Angew. Chem. Int. Ed.*, **43**, 3644 (2004).
[2] Z.Q. Xu, L.K. Thompson, C.J. Matthews, D.O. Miller, A.E. Goeta, J.A.K. Howard. *Inorg. Chem.*, **40**, 2446 (2001).
[3] J. Klingele, J.F. Boas, J.R. Pilbrow, B. Moubaraki, K.S. Murray, K.J. Berry, K.A. Hunter, G.B. Jameson, P.D.W. Boyd, S. Brooker. *Dalton Trans.*, 633 (2007).
[4] S.R. Parsons, L.K. Thompson, S.K. Dey, C. Wilson, J.A.K. Howard. *Inorg. Chem.*, **45**, 8832 (2006).
[5] C.J. Matthews, K. Avery, Z.Q. Xu, L.K. Thompson, L. Zhao, D.O. Miller, K. Biradha, K. Poirier, M.J. Zaworotko, C. Wilson, A.E. Goeta, J.A.K. Howard. *Inorg. Chem.*, **38**, 5266 (1999).
[6] Z.Q. Xu, L.K. Thompson, C.J. Matthews, D.O. Miller, A.E. Goeta, J.A.K. Howard. *Inorg. Chem.*, **40**, 2446 (2001).
[7] T.S.M. Abedin, L.K. Thompson, D.O. Miller, E. Krupicka. *Chem. Commun.*, 708 (2003).

[8] H. Grove, T.L. Kelly, L.K. Thompson, L. Zhao, Z.Q. Xu, T.S.M. Abedin, D.O. Miller, A.E. Goeta, C. Wilson, J.A.K. Howard. *Inorg. Chem.*, **43**, 4278 (2004).
[9] Y.S. Moroz, Ł. Szyrwiel, S. Demeshko, H. Kozłowski, F. Meyer, L.O. Fritsky. *Inorg. Chem.*, **49**, 4750 (2010).
[10] C.J. Matthews, L.K. Thompson, S.R. Parsons, Z.Q. Xu, D.O. Miller, S.L. Heath. *Inorg. Chem.*, **40**, 4448 (2001).
[11] V.A. Milway, V. Niel, T.S.M. Abedin, Z.Q. Xu, L.K. Thompson, H. Grove, D.O. Miller, S.R. Parsons. *Inorg. Chem.*, **43**, 1874 (2004).
[12] J. Rojo, F.J. Romero-Salguero, J.M. Lehn, G. Baum, D. Fenske. *Eur. J. Inorg. Chem.*, 1421 (1999).
[13] X.-Y. Cao, J. Harrowfield, J. Nitschke, J. Ramírez, A.M. Stadler, N. Kyritsakas-Gruber, A. Madalan, K. Rissanen, L. Russo, G. Vaughan, J.M. Lehn. *Eur. J. Inorg. Chem.*, 2944 (2007).
[14] A. Gupte, H.I. Boshoff, D.J. Wilson, J. Neres, N.P. Labello, R.V. Somu, C.G. Xing, C.E. Barry III, C.C. Aldrich. *J. Med. Chem.*, **51**, 7495 (2008).
[15] *SAINT, Program for Data Extraction and Reduction*, Bruker AXS, Inc., Madison, WI (2001).
[16] G.M. Sheldrick. *SHELXS-97, Program for the Solution of Crystal Structures*, University of Göttingen, Germany (1997).
[17] G.M. Sheldrick. *SHELXS-97, Program for Refinement of Crystal Structures*, University of Göttingen, Germany (1997).
[18] M. Kuriakose, M.R. Prathapachandra Kurup, E. Suresh. *Polyhedron*, **26**, 2713 (2007).
[19] S. Padhyé. *Coord. Chem. Rev.*, **63**, 127 (1985).
[20] C.E. Marjo, M.L. Scudder, D.C. Craig, R. Bishop. *J. Chem. Soc., Perkin Trans.*, **2**, 2099 (1997).
[21] M. Mascal. *Chem. Commun.*, 303 (1998).
[22] P.K. Thallapally, A. Nangia. *Cryst. Eng. Comm.*, **3**, 114 (2001).
[23] S.X. Liu, S. Lin, B.Z. Lin, C.C. Lin, J.Q. Huang. *Angew. Chem. Int. Ed.*, **40**, 1084 (2001).
[24] S.K. Dey, L.K. Thompson, L.N. Dawe. *Chem. Commun.*, 4967 (2006).
[25] T. Kawamoto, B.S. Hammes, R. Ostrander, A.L. Rheingold, A.S. Borovik. *Inorg. Chem.*, **37**, 3424 (1998).
[26] T. Steiner. *Angew. Chem. Int. Ed.*, **41**, 48 (2002).
[27] L.K. Thompson, C.J. Matthews, L. Zhao, Z.Q. Xu, D.O. Miller, C. Wilson, M.A. Leech, J.A.K. Howard, S.L. Health, A.G. Whittaker, R.E.P. Winpenny. *J. Solid State Chem.*, **159**, 308 (2001).
[28] C. Qin, X.L. Wang, Y.F. Qi, E.B. Wang, C.W. Hu, L. Xu. *J. Solid State Chem.*, **77**, 3263 (2004).
[29] P. Domiano, A. Musatti, M. Nardelli, C. Pelizzi. *J. Chem. Soc., Dalton Trans.*, 295 (1975).
[30] D. Kovala-Demertzi, A. Galani, M.A. Demertzis, S. Skoulika, C. Kotoglou. *J. Inorg. Biochem.*, **98**, 358 (2004).
[31] D. Kovala-Demertzi, A. Tbeodorou, M.A. Demertzis, C.P. Raptopoulou. *J. Inorg. Biochem.*, **65**, 151 (1997).